Alteration of the Serum *N*-glycome of Mice Locally Exposed to High Doses of Ionizing Radiation*[S]

Thibault Chaze‡§, Marie-Christine Slomianny§¶, Fabien Milliat‡, Georges Tarlet‡, Tony Lefebvre-Darroman¶, Patrick Gourmelon‖, Eric Bey, Marc Benderitter‡, Jean-Claude Michalski¶, and Olivier Guipaud‡‡‡**

Exposure of the skin to ionizing radiation leads to characteristic reactions that will often turn into a pathophysiological process called the cutaneous radiation syndrome. The study of this disorder is crucial to finding diagnostic and prognostic bioindicators of local radiation exposure or radiation effects. It is known that irradiation alters the serum proteome content and potentially post-translationally modifies serum proteins. In this study, we investigated whether localized irradiation of the skin alters the serum glycome. Two-dimensional differential in-gel electrophoresis of serum proteins from a man and from mice exposed to ionizing radiation showed that potential post-translational modification changes occurred following irradiation. Using a large-scale quantitative mass-spectrometry-based glycomic approach, we performed a global analysis of glycan structures of serum proteins from non-irradiated and locally irradiated mice exposed to high doses of γ-rays (20, 40, and 80 Gy). Non-supervised descriptive statistical analyses (principal component analysis) using quantitative glycan structure data allowed us to discriminate between uninjured/slightly injured animals and animals that developed severe lesions. Decisional statistics showed that several glycan families were down-regulated whereas others increased, and that particular structures were statistically significantly changed in the serum of locally irradiated mice. The observed increases in multiantennary N-glycans and in outer branch fucosylation and sialylation were associated with the up-regulation of genes involved in glycosylation in the liver, which is the main producer of serum proteins, and with an increase in the key proinflammatory serum cytokines IL-1β, IL-6, and TNFα, which can regulate the expression of glycosylation genes. Our results suggest for the first time a role of serum protein glycosylation in response to irradiation. These protein-associated glycan structure changes might signal radiation exposure or effects. ***Molecular & Cellular Proteomics 12: 10.1074/mcp.M111.014639, 283–301, 2013.***

Radiation-induced damage to the skin layer is complex and leads to a defined variety of specific reactions that often turn into a pathophysiological process known as the cutaneous radiation syndrome (CRS)[1] (1–3). High doses of ionizing radiation induce reactions that arise from days to years afterward and which can reach different grades of severity, such as erythema, dry and moist desquamation, ulceration, and necrosis (4). Reports on different radiation accidents have clearly shown that skin damage can determine the prognosis and outcome of the whole-body reaction (5), emphasizing the fact that it is crucial to manage the consequences of local irradiation and to predict as early as possible the severity of future lesions.

The severity of radiation-induced reactions depends on the dose received, but not exclusively. In particular, the severity of lesions induced by local exposure will greatly depend on the extent of the surface area and on the volume exposed to radiation. Advanced techniques focusing on different cytogenetic, genetic, physical, and immunohistochemical parameters are used to estimate the dose received (6). However, these techniques are more appropriate for whole-body irradiation than for localized exposure, need to be performed by skilled people, and mostly are time consuming. Also, even if it is possible to diagnose a radiation burn, predicting the outcome of a lesion remains difficult, especially when the lesion is localized. Among different available therapeutic strategies

From the ‡Institut de Radioprotection et de Sûreté Nucléaire (IRSN), DRPH, SRBE, LRTE, 92260 Fontenay-aux-Roses, France; ¶Unité de Glycobiologie Structurale et Fonctionnelle, UMR8576, Université des Sciences et Techniques de Lille, 59655 Villeneuve D'Ascq, France; ‖Institut de Radioprotection et de Sûreté Nucléaire (IRSN), DRPH, 92260 Fontenay-aux-Roses, France; **Hôpital d'Instruction des Armées Percy, 92140 Clamart, France

Received October 20, 2011, and in revised form, November 8, 2012
Published, MCP Papers in Press, November 12, 2012, DOI 10.1074/mcp.M111.014639

[1] The abbreviations used are: ANOVA, analysis of variance; APP, acute phase protein; Co, cobalt; CRS, cutaneous radiation syndrome; DIGE, differential in-gel electrophoresis; Gy, Gray; Ig, immunoglobulin; IL, interleukin; Ir, iridium; MeV, mega-electron-volt; NP40, Nonidet P40; PB, phosphate buffer; PCA, principal component analysis; p*I*, isoelectric point; PMMA, polymethyl methacrylate; PNGase F, peptide: *N*-glycosidase F; SLe^x, sialyl Lewis X; TGFβ, transforming growth factor β; TNFα, tumor necrosis factor α.

for local injury, stem-cell-based therapies are very promising (7–10). Nevertheless, the use of such therapies needs to be anticipated as early as possible in order to allow enough time to isolate and amplify cells before treatment. Therefore, new tools still have to be discovered to enable better prediction of the severity of localized injuries. These markers will help clinicians make the right decisions in a timely manner and choose the most suitable therapeutic strategy.

Proof of principle for using different sets of proteins as indicators of exposure has been established in a few studies (11, 12), but no indicator has been proposed for the diagnosis or prognosis of localized skin injury. Among classic laboratory tests, those based on blood sampling are semi-invasive, are high-throughput, and can be automated, so they may be used for the assessment of radiation dose and/or the prediction of radiation effects. Blood composition is modified after exposure to ionizing radiation through the immediate release by irradiated cells of cytokines and growth factors that stimulate neighboring cells or distant cells, which in turn release proteins in the extracellular environment. IL-1, IL-6, IL-8, TGFβ, TNFα, and eotaxin are the major known cytokines involved in the response of the skin and skin cells to ionizing radiation (13, 14). Cytokines play a role in mediating the inflammation process and stimulate or repress acute phase protein (APP) synthesis in the liver (15), assisting the repair of the tissue. This inflammation process that occurs following localized radiation injury is a complex and in part specific mechanism that is only beginning to be elucidated. Investigations of the quantitative (expression levels) and qualitative (post-translational modifications) changes of blood proteins are therefore crucial if we are to understand radiation-induced inflammation and discover new bioindicators of radiation exposure and radiation effects.

As applied to radiation biology, omics are interesting approaches suitable for discovering biomarker candidates and describing pathways involved in the response to ionizing radiation, giving rise to a new understanding of pathophysiological modifications (11). Using two-dimensional differential in-gel electrophoresis (DIGE) coupled with mass spectrometry, we have shown that the serum proteome content is deeply altered from 1 day to 1 month following exposure of the skin to high doses of ionizing radiation (16). Moreover, we observed shifts in the isoelectric point (p*I*) of several proteins, revealing potential post-translational modification changes after irradiation, conceivably due to changes in the glycan structures carried by these proteins.

Protein glycosylation is one of the most common post-translational modifications of secreted proteins (17); half of all proteins are thought to be glycosylated (18). Changes in a particular glycoform can induce several physiological modifications and might turn out to be a signature of a particular disease (19). Among glycoform types, *N*- and *O*-glycans have been studied most. *N*-glycosylation (linkage of the glycan to asparagine through a consensus sequence) is the most abundant modification of serum proteins. *O*-glycosylation (the glycan is attached to serine or threonine through an acyl linkage) is very common in mucins, proteoglycans, and collagens, but not in serum. The whole glycosylated status of tissues, cells, or body fluids can be studied using emerging glycomic and glycoproteomic tools (20), whose great potential for deepening our understanding of diseases and for aiding in the discovery of new biomarkers is now clearly established (21–24). This contribution is essentially the result of technical advances made through mass-spectrometry-based investigations (25, 26).

Given that glycosylation status and inflammation are closely linked (27), and that glycosylation (28) and localized irradiation of the skin of mice (16) both induce major shifts in the p*I* of serum proteins on two-dimensional gel electrophoresis, we addressed the question of whether skin irradiation alters the glycome using a large-scale mass-spectrometry-based glycomic approach. We show here that the expression of various glycan structures was modified in the serum of mice exposed locally to high doses of ionizing radiation, suggesting a role of glycosylation in the response to irradiation. To our knowledge, this is the first study describing the modification of the total serum *N*-glycome following exposure to ionizing radiation.

EXPERIMENTAL PROCEDURES

Patient and Irradiation Accident—A 27-year-old Chilean man was overexposed on December 15, 2005, to a gammagraphy radioactive source of ^{192}Ir (3.3 TBq). Following multifocal localized irradiation, he rapidly exhibited severe radiation burns on the hand and buttock, as described elsewhere (7).

Human Biological Sampling and Affinity Depletion of High Abundance Proteins—Blood (5 ml) was collected from the Chilean man 22 days after irradiation (Hôpital d'Instruction des Armées Percy, Clamart, France), as well as from 12 healthy volunteer donors (Service de Santé au Travail, CEA/IRSN, Fontenay-aux-Roses, France), in plastic serum tubes (BD Vacutainer SST advance tubes, BD Biosciences). After sitting for 1 h at room temperature, blood was centrifuged at 1000 $\times$ *g* for 10 min at 4 °C, and the supernatant was collected. Serum was then stored at −80 °C. Serum samples (20 μl) were processed using a human Multiple Affinity Removal Spin Cartridge (Agilent Technologies, Massy, France), which selectively removed human albumin, IgG, IgA, haptoglobin, α1-antitrypsin, and transferrin proteins, as described elsewhere (16). Protein concentrations were determined by means of the Bradford assay (Bio-Rad). Four technical replicates were performed for the serum of the Chilean man. All healthy donors gave written consent for blood collection (consent form number 09001) in accordance with current French regulations. Blood samples from the Chilean patient were obtained within the framework of his treatment at Percy Hospital. The patient gave written consent for a new therapeutic strategy combining a surgical approach and mesenchymal stem cell local therapy; ethical and technical approvals were obtained from the French Agency for the Safety of Health Products (7).

Animals—Male mice (BALB/c, 8 weeks old, Janvier, Le Genest Saint Isle, France) were used in this study. Experimental procedures were approved by the animal care committee of the French Institute of Radiological Protection and Nuclear Safety (institutional review board approval number P09–19) and were conducted according to the French regulations for animal experimentation (Ministry of Agri-

culture, Act No. 2001–464, May 29, 2001). Mice were housed 4 per cage and received rodent chow and water *ad libitum*.

Dorsal Skin Irradiation of Mice—The irradiation protocol used in this study is mostly the same as that previously published (16). Mice were irradiated at different doses (20, 40, and 80 Gy, 8 mice per dose), and control mice were sham-irradiated (8 mice). Two days before irradiation, hair from the entire back of the mouse was removed using an electric shaver. Mice were anesthetized via spontaneous inhalation of isoflurane-N_2O gas (Forene, Abbott GmbH) and irradiated using 1.25 MeV γ-rays from a collimated ^{60}Co source (dose rate of 1.4 Gy/min). The dorsal skin was gently stretched and maintained on a 4-mm-thick polymethyl methacrylate (PMMA) plate with two suturing lines. The reference dose rate was established with an ionization chamber (PTW, Freiburg, Germany) in realistic irradiation conditions in air on the PMMA plate with a tissue equivalent phantom at mouse body position to generate back-scattered radiation from the mouse bodies. The 0.125-cm^3 PTW ionization chamber was calibrated in terms of tissue kerma at the Institut de Radioprotection et de Sûreté Nucléaire reference ^{60}Co facility (accredited metrological unit SMH, no. 2–1612, COFRAC accreditation, France).

Mouse Skin Lesion Scoring System—Skin lesions were scored daily using a scale described elsewhere (16). Briefly, the lesions were scored as follows: 0, normal; 0.5–1, slight to intense erythema; 1–1.5, dry desquamation; 1.5–2.5, moist desquamation (less than 50% of the irradiated area); 2.5–3, a few spots of necrosis in addition to between 50% and 100% moist desquamation; 3–3.5, several zones of necrosis in addition to 100% moist desquamation; and 3.5, necrosis of the entire irradiated area.

Mouse Biological Sampling—Blood (100 μl per animal) was collected from the orbital sinus of anesthetized mice (spontaneous inhalation of isoflurane-N_2O gas) 7 or 14 days after irradiation. After 30 min at room temperature, blood was centrifuged at 1000 $\times$ *g* for 10 min at 4 °C, and the supernatant was collected. Serum was then stored at −80 °C.

Affinity Depletion of High Abundance Proteins for Two-dimensional DIGE Analysis—For two-dimensional DIGE analysis, serum samples (20 μl each, 8 mice per dose of irradiation) were processed using a mouse Multiple Affinity Removal Spin Cartridge (Agilent Technologies), which selectively and specifically removed mouse albumin, IgG, and transferrin proteins, as described elsewhere (16). A low abundance protein fraction of 400 μl was collected and 10-fold concentrated using a 3-kDa molecular weight cut-off spin concentrator (Amicon Ultra 0.5, Millipore, Molsheim, France) by means of centrifugation at 14,000 $\times$ *g* for 45 min at 20 °C. For the study of glycoprotein via two-dimensional DIGE, each sample was diluted to 500 μl with phosphate buffer (PB) containing antiproteases (Protease Inhibitor Mixture, Roche Diagnostics) and concentrated via ultrafiltration (Amicon Ultra 0.5, Millipore) at 14,000 $\times$ *g* for 50 min at 20 °C. Protein concentrations were determined by means of the Bradford assay (Bio-Rad).

Two-dimensional DIGE Experimental Design for Mouse Serum Proteins—A comparative two-dimensional DIGE approach was used with deglycosylated or native depleted mouse serum proteins after removing (or not) *N*-glycans. Each depleted sample ($n = 4$ per group) was separated into two fractions of 90 μg each and denatured by means of boiling at 100 °C for 10 min in one volume of lysis buffer (1% SDS and 2% β-mercaptoethanol in PB). After being cooled to room temperature, and after the addition of two volumes of PB with 1% Igepal (Sigma Aldrich), the fractions were incubated at 37 °C for 24 h with or without three units of peptide: *N*-glycosidase F (PNGase F) (Roche Diagnostics). Samples were finally boiled at 100 °C for 10 min to stop the enzymatic reaction. Fractions were concentrated using a 3-kDa molecular weight cut-off spin concentrator (Amicon Ultra 0.5, Millipore) by means of centrifugation at 14,000 $\times$ *g* for 45 min. Buffer exchange was performed twice via the addition of up to 500 μl of two-dimensional gel electrophoresis buffer (7 M urea, 2 M thiourea, 0.5% CHAPS, and 18 mM DTT) and centrifugation at 14,000 $\times$ *g* for 40 min. High-abundance-depleted serum proteins (50 μg) were minimally labeled with 400 pmol of Cy2, Cy3, or Cy5 DIGE fluors (GE Healthcare) as described elsewhere (16). Samples consisted of depleted serum (untreated or treated with PNGase F) from individual control mice (eight samples) and mice irradiated at 20 Gy (eight samples), 40 Gy (eight samples), and 80 Gy (eight samples). A total of 16 SDS-PAGE tests were performed, with each gel containing two different samples (Cy3- and Cy5-labeled) and an internal standard sample (Cy2-labeled). A dye-swapping scheme was used so that four samples from any condition were never labeled with Cy3 or Cy5 to avoid any specific dye-labeling artifacts that might occur.

Two-dimensional DIGE Experimental Design for Human Serum Proteins—High-abundance-depleted serum proteins (50 μg) were minimally labeled with 400 pmol of Cy2 (internal standard), Cy3, or Cy5 DIGE fluors (GE Healthcare) as described elsewhere (16). Samples consisted of depleted serum from individual healthy donors (12 samples) and from the Chilean man who had been accidentally irradiated (four technical replicate samples, 22 days post-irradiation). A total of eight SDS-PAGE tests were performed, with each gel containing two different samples (Cy3- and Cy5-labeled) and an internal standard sample (Cy2-labeled). A dye-swapping scheme was used so that samples from any condition were never labeled with Cy3 or Cy5 to avoid any specific dye-labeling artifacts that might occur.

Two-dimensional Gel Electrophoresis and Imaging—Protein samples labeled with Cy2, Cy3, and Cy5 dyes were mixed and diluted with rehydration buffer to 450 μl as described elsewhere (16). 150 μg (combination of the three labeled protein samples) of protein was applied to 24-cm-long immobilized pH 4–7 gradient strips (GE Healthcare) via the passive rehydration technique for 24 h. First-dimension isoelectric focusing (IEF) was performed using an IPGPhor 3 electrophoresis unit (GE Healthcare) cooled to 18 °C for a total of 55 kVh. After IEF, strips were equilibrated and placed on top of hand-cast SDS-containing 10% polyacrylamide gels, and SDS-PAGE was then carried out at 0.5 W per gel for 1 h followed by 1 W per gel for 16 h (Ettan DALT 12 system, GE Healthcare) as described elsewhere (16). After electrophoresis, gels were scanned directly between glass plates using a Typhoon 9400 imager (GE Healthcare).

MALDI-TOF/TOF MS Analysis of Permethylated Mouse Serum N-glycans—25 μl of raw (non-depleted) serum ($n = 7$ or 8 per group) was mixed with lysis buffer (50 mM PB, pH 7.0, containing 0.5% SDS and 1% β-mercaptoethanol) and incubated at 100 °C for 15 min. *N*-glycans were purified and analyzed as described elsewhere (25). After cooling and the addition of PB and 1% Nonidet P-40, three units of PNGase F (Roche Diagnostics) were added and samples were incubated for 24 h at 37 °C. Released glycans were purified on a graphitized carbon column (Alltech, Deerfield, FL). *N*-glycans were then permethylated as described elsewhere (29) and purified on an SPE C18 column (Alltech). Permethylated glycans were then dissolved in methanol/water (1:1 v/v) and mixed with an equal volume of dihydroxyaminobenzoic acid matrix (Aldrich) (20 mg/ml in methanol/water 1:1 v/v). Two technical replicates were performed per sample. Mass spectra were acquired using an Applied Biosystems 4800 MALDI-TOF/TOF Analyzer equipped with a neodymium-doped yttrium aluminum garnet laser of wavelength 335 nm. MALDI spectra were recorded solely in the positive ion mode, as permethylation eliminates the negative charge normally associated with sialylated glycans. Spectra were obtained through the accumulation of 1500 laser shots over an *m/z* range of 1500–5000 Da. The two technical replicates were spotted on the MALDI target plate, and two spectra were acquired per spot, giving rise to a total of four spectra per sample. Spectra were calibrated using an external standard composed of bradykinin fragment 1–7 ($M + H^+ = 757.399$), angiotensin II

(human) ($M + H^+ = 1046.542$), P14R (synthetic peptide) ($M + H^+ = 1533.858$), ACTH fragment 18–39 (human) ($M + H^+ = 2465.198$), and insulin oxidized B chain (bovine) ($M + H^+ = 3494.651$) (MSCAL2, Sigma Aldrich). With MALDI-TOF/TOF, the mass tolerance for precursor ions is specified by a range based on the resolution of the precursor mass. Here, the relative mass window was fixed at a value of 200. The MS/MS data were searched with a mass tolerance of 500 ppm.

Data Evaluation and Statistical Analysis—For two-dimensional DIGE analysis, scanned gels were analyzed with Progenesis SameSpot software, version 4.1 (NonLinear Dynamics, Durham, NC). The differential in-gel analysis module was used to compare quantitatively the normalized volume ratio of each individual protein spot-feature from a Cy3- or Cy5-labeled sample on a given gel relative to the Cy2-signal from the pooled sample standard corresponding to the same spot feature. Within each gel, the co-resolved fluorescent signals from each protein were co-detected by the software, and abundance measurements were made directly of the internal standard without interference from gel-to-gel variation. One-way analysis of variance (ANOVA) was performed with SameSpot software and was used to calculate significant differences in the relative abundances of proteins from control and irradiated mice and in glycosylated and deglycosylated sera. Principal component analysis (PCA) of two-dimensional DIGE quantitative data was performed using the statistical module of the Progenesis SameSpot software and was used in interpreting relationships between experimental groups.

For MALDI-TOF analysis, the MS profiles of permethylated *N*-glycans were further processed using Data Explorer, version 4.7, to generate ASCII files containing *m/z* values and signal intensities after calibration, smoothing, and deisotoping function. For each *m/z* value, the peak intensities of the four acquired spectra per sample were averaged prior to further analysis. The processing method was chosen to filter peaks based on the signal-to-noise (S/N) ratio using an S/N ratio threshold of 3. Furthermore, the processing method took into account isotopic distributions to recalculate S/N ratios in order to finally eliminate those under 10. The mass lists and their corresponding peak intensities (raw data) are given in supplemental Table S1. GlycoWorkBench, version 2.0 alpha, from EUROcarbDB (30), which encloses the GlycomeDB database for carbohydrate structures (35,873 unique carbohydrate sequences) (31), was used to establish our own glycan database from mouse samples, to annotate MALDI-MS and MALDI-MS/MS spectra, and to propose putative glycan structures. Thirty-nine different ions were finally selected as possible glycan species according to the following criteria: good reproducibility of the signal between the four acquired spectra per sample and between samples (absence or few null values), the presence of a probable corresponding structure in the EUROcarbDB database, S/N ratios over 10, and confirmation of the putative structure via MALDI-TOF/TOF tandem mass spectrometry. Annotated MALDI-MS/MS spectra are displayed in supplemental Fig. S1. Each monoisotopic signal was assigned to a monosaccharide composition and further classified in different families: high mannose, complex, hybrids, and *N*-acetylhexosamine-ended species. Complex-type *N*-glycans were then subdivided into several subfamilies for evaluation of antennary rate and terminal glycosylation (21). The relative proportion (percent intensity) of each structure or family was calculated as (intensity $\times$ 100)/(sum of intensities). Supplemental Table S2 displays all MALDI-TOF-MS signal intensities and percent intensities for each *m/z* value of our glycan database and for each acquisition. Normality and equal variance were assessed with percentage intensity data prior to the use of one-way ANOVA to compare the four series of data for each structure or family. The one-way ANOVA on ranks (Kruskal–Wallis) test was used in cases when the normality or the equal variance test failed. All pairwise multiple comparison procedures (Tukey's test and Dunn's method) were used, respectively, only when ANOVA or ANOVA on ranks *p* values were less than 0.05. All statistical tests were performed with SigmaPlot software, version 11, and are presented in supplemental Tables S3 and S4. PCA was performed with the package FactoMineR (32) to visualize and highlight better the similarities between individuals.

RNA Isolation, Reverse Transcription, and Real-time Quantitative PCR—Total RNA from mouse liver (20 to 25 mg, 8 mice per dose and per time point post-irradiation) kept at -20 °C in RNAlater buffer (Qiagen) was prepared with the total RNA isolation kit (RNeasy Mini Kit, Qiagen, Courtaboeuf, France). RNA quantification and integrity were analyzed using a Nanodrop spectrophotometer ND-1000 (LabTech, Palaiseau, France) and an Agilent 2100 bioanalyzer. Reverse transcription was performed with 1 μg of total RNA using a reverse transcription kit from Applied Biosystems (Villebon sur Yvette, France). Pre-developed TaqMan gene expression assays (Applied Biosystems) were used to quantify transcript levels of all studied genes (supplemental Table S5). Quantitative PCR was carried out using the ABI PRISM 7900 sequence detection system, and the results were normalized to the housekeeping genes GAPDH or 18S. Relative mRNA levels were quantified using the $\Delta\Delta$CT method. Data are presented as mean $\pm$ S.E. and are expressed relative to the corresponding control (non-irradiated) sample values. Student's *t* test, or the Mann–Whitney test when the normality or the equal variance test failed, was used to compare values with SigmaPlot software, version 11 (supplemental Table S6). For all analyses, a *p* value < 0.05 was taken as significant.

Multiplexed Cytokine Analysis—Cytokine concentrations in the serum were assayed using a mouse magnetic 3-plex cytokine kit (Bio-Rad) (8 mice per dose and per time point post-irradiation). The kit can simultaneously quantify three mouse cytokines and chemokines: IL-1β, IL-6, and TNFα. The assay was performed according to the manufacturer's protocol. After preparation, samples were processed (50 beads per bead set in 50-μl sample size) on a Bio-Plex 200 instrument (Bio-Rad). All the samples were run in duplicate. The data were analyzed using Bio-Plex Manager 6.0 software. For each assay, a standard curve was generated for detection from 3.14 pg/ml to 51,408 pg/ml (IL-1β), 1.34 pg/ml to 21,960 pg/ml (IL-6), and 2.73 pg/ml to 44,662 pg/ml (TNFα). Data are presented as mean $\pm$ S.E. Student's *t* test, or the Mann–Whitney test in the case when the normality or the equal variance test failed, was used to compare values with the SigmaPlot software, version 11. For all analyses, a *p* value < 0.05 was taken as significant.

RESULTS

Scoring of Irradiated Mouse Lesions—An experimental model of CRS was previously established by selectively irradiating the dorsal skin of BALB/c mice (16, 33). We used this model by irradiating mice at 20, 40, and 80 Gy to induce, respectively, erythema, dry desquamation, and necrosis of the skin in the course of the development of the lesion. As previously observed, lesions developed from the seventh day post-irradiation whatever the dose of ionizing radiation (Fig. 1). They evolved from erythema (score: 0.5–1) to necrosis (score: 3–3.5) as a function of time and dose of ionizing radiation, reaching a peak around 3 weeks following exposure. Slow wound healing took place over different times depending on the exposure dose. At day 14 post-irradiation, the animals irradiated at 40 and 80 Gy presented lesions still in an active growth phase but displaying about the same scores, while the lesions evolved toward different maximum

intensities, suggesting that this time point might be interesting for the discovery of factors predictive of the evolution of an established lesion. We observed in our first study that maximum proteome changes occurred at day 14, whereas the maximum intensity of the lesion was noted at around 21 days post-irradiation (16). The time point of day 14 could thus be of interest for observing major changes in the glycome content of serum proteins. For these reasons, we chose to study mouse glycome changes at day 14 post-irradiation.

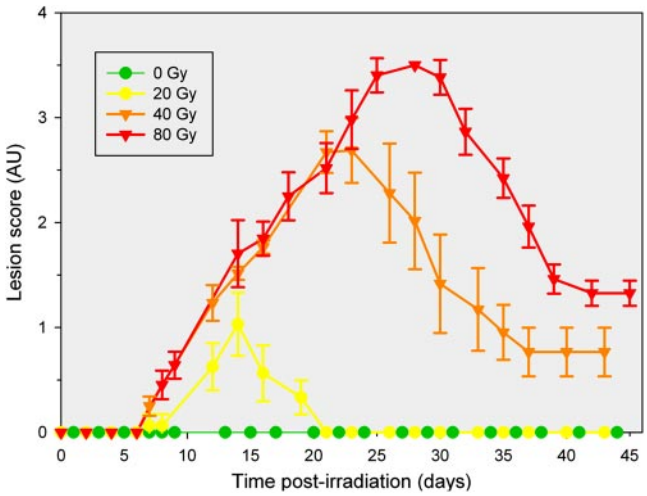

FIG. 1. **Evolution of skin lesions in mice following irradiation at different doses (*n* = 8 per group; mean ± S.E. in arbitrary units (AU)).**

Human and Mouse Serum Two-dimensional DIGE Profiles during CRS—Two-dimensional DIGE methodology was used to study serum proteome profiles in order to confirm first observations that some protein spot trains shifted mainly toward acidic pH values after irradiation, suggesting post-translational modification changes (16). We also used the same methodology for serum proteins from an accidentally locally irradiated man who was developing CRS at the time of blood collection (22 days after exposure) (7). Figs. 2*A* and 2*B* show that proteome profiles of human and mouse sera displayed closely related changes relative to serum proteins from control individuals (over- and underexpressed spots appear in red and green, respectively). In particular, it can be seen that many proteins from the human serum formed spot trains, and several of them shifted toward acidic pH values, as observed in mouse samples. Such spot trains displayed three different colors on the merged image of the two initial scans, showing that the spot train from one condition is displaced relative to the spot train of the other condition (attested to by the two different colors of the two different cyanines in addition to the color of the merged image of the two colors). Examples of such spot trains are given in Figs. 2*C* and 2*D*, in which spot

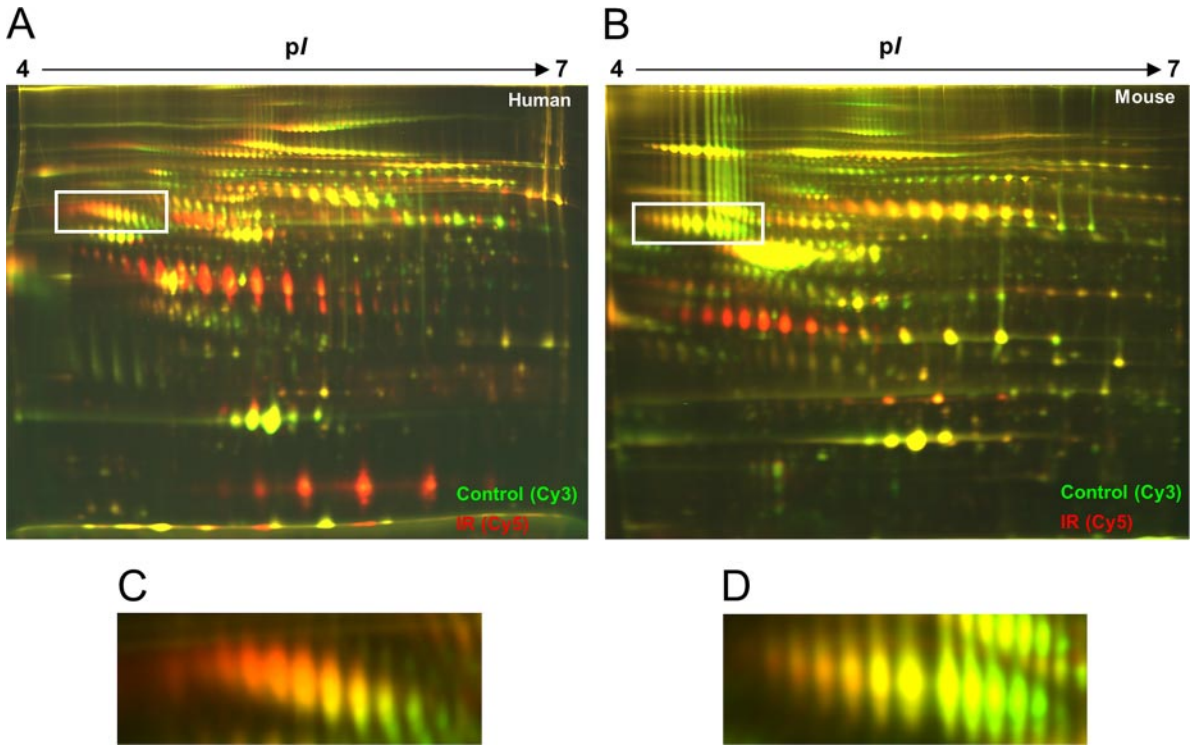

FIG. 2. **Two-dimensional difference gel electrophoresis analysis of serum proteins from skin-irradiated mice and a man locally irradiated by accident.** *A*, serum proteins from a healthy volunteer (Cy3-labeled, green) and the irradiated man (Cy5-labeled, red) 22 days following strong local irradiation (merged image of the two scanned gels). *B*, serum proteins from control (Cy3-labeled, green) and irradiated (Cy5-labeled, red) mice 14 days after irradiation of the skin at 80 Gy (merged image of the two scanned gels). *C*, *D*, magnified image of the delimited areas (outlined by white rectangles) presented in panels *A* and *B*, respectively.

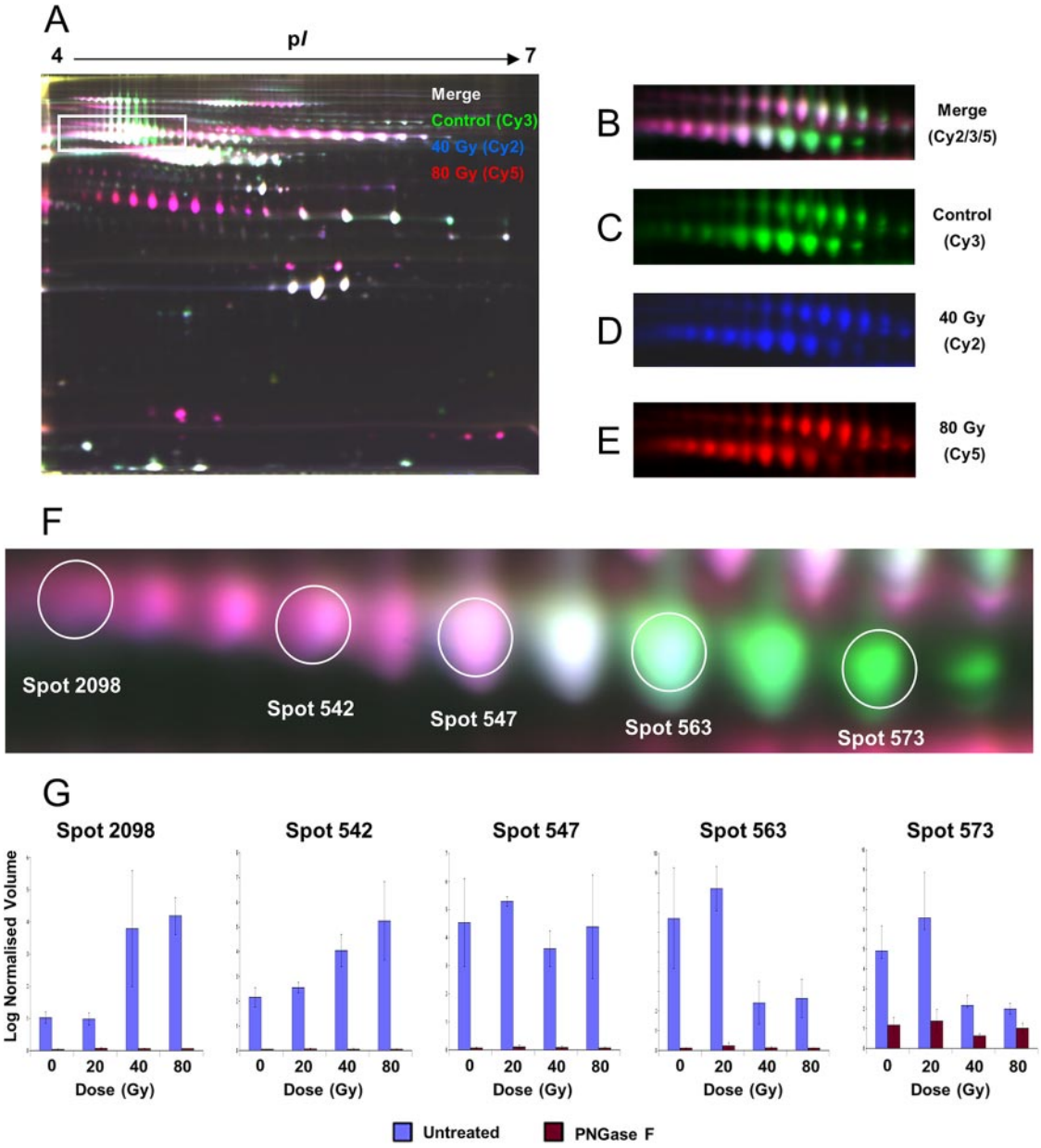

FIG. 3. **The magnitude of shifts of spot trains toward acidic pH levels is dose dependent in mouse, and proteins of spot trains are glycosylated.** *A*, serum proteins from control mice (Cy3-labeled, green) and mice irradiated at 40 Gy (Cy2-labeled, blue) and 80 Gy (Cy5-labeled, red) 14 days after irradiation of the skin (merged image of the three scanned gels). *B–F*, magnified images of the delimited area (outlined by a white rectangle) presented in panel *A*: *B* and *F* represent the merged images of the three scanned gels, and *C*, *D*, and *E* present the single images (Cy3, Cy2, and Cy5, respectively). *G*, quantification of the levels of the different spots contained in the spot train presented in panel *F* in untreated and in PNGase F–treated serum samples.

trains display red on one side, green on the other, and yellow in the middle. This interpretation has been stated in detail previously (16). We then addressed the question of whether the location of spot trains on two-dimensional gel electrophoresis could be dependent on the dose of irradiation. Three different sera from control and irradiated animals were labeled with the three fluorescent cyanine dyes Cy3 (sham-irradiated, $n = 4$), Cy2 (40 Gy, $n = 4$), and Cy5 (80 Gy, $n = 4$), and were run 3 × 3 on the same gel (Fig. 3). In this case, we observed that some spot trains—for instance, the one presented in Figs. 3*B*–3*E*, which was identified as contrapsin (serpina 3K) via mass spectrometry fingerprinting in our previous study (16)—were made up of four dominant colors: red, pink (a mixture of blue and red), white (a mixture of blue, red, and green), and green, from acidic pH to basic pH. This result confirmed the changes we observed between two samples (control and irradiated individuals, Fig. 2). Mean relative quantities of the different spots of the contrapsin spot train were

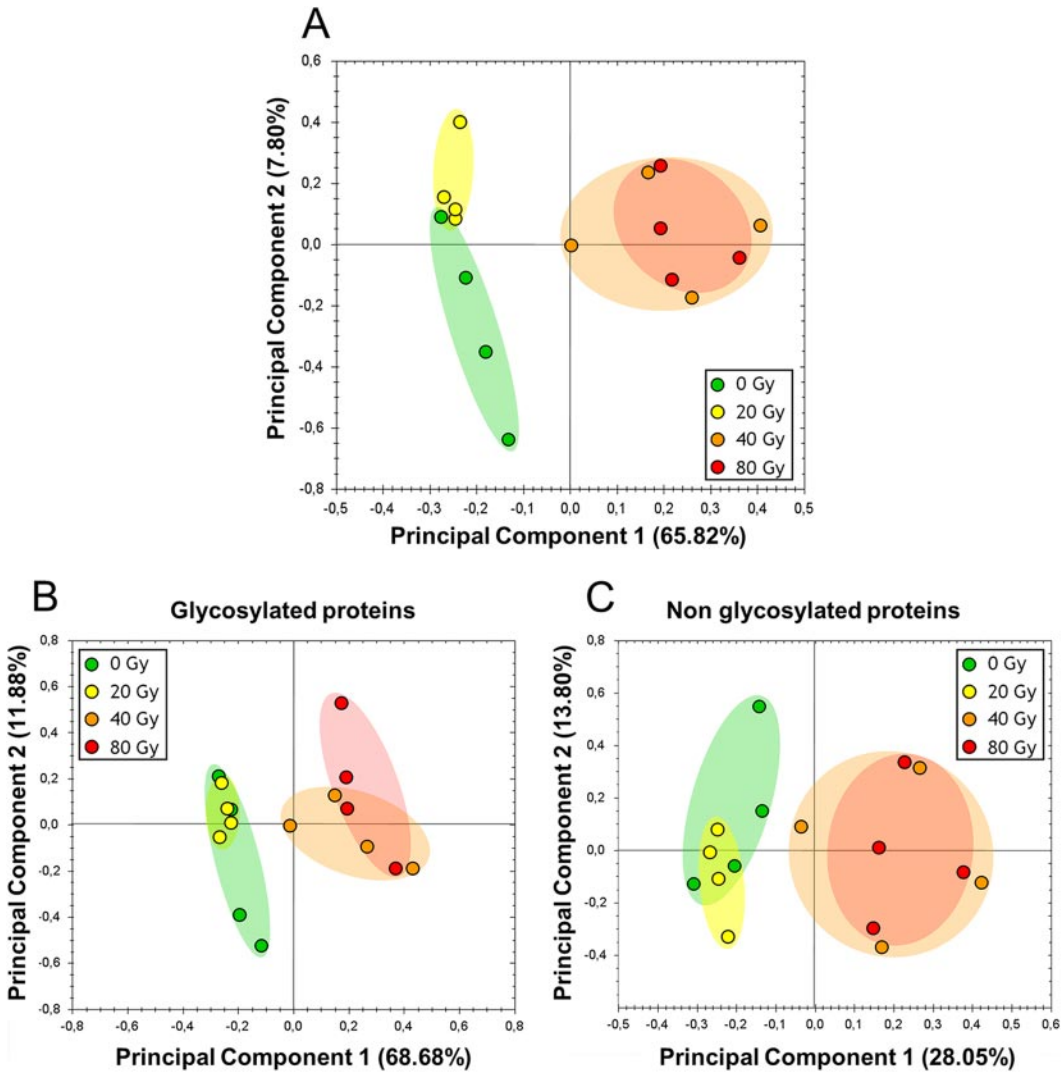

FIG. 4. **Principal component analysis of two-dimensional DIGE spots derived from control mice (n = 4) and mice irradiated at 20 Gy (n = 4), 40 Gy (n = 4), and 80 Gy (n = 4).** *A*, all differentially expressed two-dimensional DIGE spots. *B*, glycosylated two-dimensional DIGE spots. *C*, unglycosylated two-dimensional DIGE spots.

evaluated using Progenesis SameSpots software, demonstrating that the more acidic spot increased with the dose of irradiation, whereas the more basic spot decreased (Figs. 3*F* and 3*G*). Interestingly, the treatment of serum samples with PNGase F markedly changed two-dimensional gel electrophoresis protein profiles whatever the dose of irradiation and allowed the complete disappearance of the contrapsin spot train presented in Fig. 3*F*, as attested to by the relative quantification of each spot of the spot train (Fig. 3*G*). This strongly suggests that all spots of the contrapsin spot train were modified by *N*-glycans. Taken together, these results show that the shift of spot trains toward acidic pH is dependent on the dose of irradiation, suggesting that the more the dose is increased, the greater the modification of the protein is. Because these modifications could be due to changes in *N*-glycosylation, we further investigated abundance changes in these post-translational modifications.

Two-dimensional DIGE Analysis of Glycosylated and Deglycosylated Mouse Serum Proteins—In order to evaluate the contribution of glycan moieties to the discrimination of samples from control and irradiated mice, profiles of high-abundance-protein-depleted serum treated (or not) with PNGase F were compared using a two-dimensional DIGE approach. A total of 733 protein spots were detected in the reference gel, which was constituted by a merged image of all sham-irradiated, irradiated, non-treated, and PNGase F–treated samples. The contribution of glycans branched on protein cores was analyzed using PCA, which gave a simplified view of gel data in a two-parameter map. Firstly, PCA was performed using only proteins exhibiting a p value under 5% given by ANOVA of all groups of serum proteins not treated with PNGase F (Fig. 4*A*). This allowed good clustering of animals in two main groups, as the first principal component (PC1) explained about 66% of data variability: controls and animals irradiated

at 20 Gy, and animals irradiated at 40 Gy and 80 Gy. Analysis of profiles of serum proteins deglycosylated with PNGase F allowed the selection of 74 proteins assumed to be *N*-glycosylated because their spot volumes turned null after the treatment. Once again, PCA for these 74 proteins allowed good clustering of two main groups, as PC1 explained 68% of the observed variability: controls and animals irradiated at 20 Gy, and animals irradiated at 40 and 80 Gy (Fig. 4*B*). In order to evaluate the contribution of proteins that were not affected by the PNGase F digestion in terms of electrophoretic mobility (*i.e.* thought to be non-*N*-glycosylated), we then performed PCA using only protein spots whose volumes did not change after the PNGase F treatment. The PCA plot displayed once again the same two clusters as observed in the two other PCA plots, but PC1 decreased to 28% of the variance (Fig. 4*C*). This suggested the importance of serum protein glycosylation changes, or changes in the abundance of serum glycosylated proteins, in explaining the discrimination between control–20 Gy and 40–80 Gy samples.

Mass Spectrometry Glycan Profile Analysis—Because glycan moieties seemed to be important in explaining proteome changes during CRS in mice, we focused on the analysis of glycan modifications at day 14 post-irradiation. MS-based analytical strategies offer highly sensitive and very informative tools that can be used to address the complexity of the structural analysis of glycans. The pilot study conducted by the Human Proteome Organization and the Human Disease Glycomics/Proteomics Initiative revealed the high reproducibility of MS analysis of permethylated *N*-glycans resulting in good quantitation of oligosaccharide mixtures in MALDI-MS (34). We used a comparative glycomic approach that allowed quantitative distinction between the glycan structures derived from whole (non-depleted) sera of control animals and animals irradiated at 20, 40, and 80 Gy ($n = 7$ or 8 per group). Profiles of permethylated glycans derived from 25 μl of raw serum were recorded for the *m/z* range of 1500–5000 Da using MALDI-MS (seven or eight biological replicates, two technical replicates per biological replicate, and two spectrum acquisitions per technical replicate) (supplemental Tables S1 and S2). Thirty-nine different ions were finally selected as possible glycan species according to the following criteria: good reproducibility of the signal between the four acquired spectra per sample and between samples (absence or few null values), the presence of a probable corresponding structure in the EUROcarbDB database, S/N ratios over 10, and confirmation of the putative structure via MALDI-TOF/TOF tandem mass spectrometry that allowed composition assignment of the different glycans and classification in different families (supplemental Fig. S1). For instance, some ions were actually not considered in the study because they were unlikely to be *N*-glycan structures, or because their intensities were too variable between the four acquired spectra per sample. The 39 structures are listed in Table I, which also displays putative schematic structures determined after MS/MS analysis by MALDI-TOF-TOF and using GlycoWorkBench software. The presented putative structures were determined on the basis of composition, biosynthetic pathway knowledge, and MS/MS fragmentations. However, MALDI-MS/MS was not able to differentiate isomers. For convenience, only one branching pattern for triantennary structures and one branching pattern for hybrid structures are shown. *N*-acetyl and *N*-glycolylneuraminic acids were observed in serum samples from mice. The higher observed *m/z* corresponded to a tetraantennary fucosylated glycan (*m/z* value of 4084). Fig. 5 illustrates representative glycan map profiles of control and 80-Gy-irradiated mouse serum proteins and shows qualitatively similar profiles but different peak intensities between the two samples. Changes in relative abundances of structure species observed in glycosylation patterns between control and irradiated animals were further determined using decisional statistics (see below). All generated maps displayed the same broad profile whatever the dose received by the mice, as expected for good data interpretation (34). Mean coefficients of variation of the different structures, including biological and technical variations, were calculated as around 28% (from 26% to 30%) within each group, close to those of standard proteomic studies (35–38). Profiles of control samples generally appeared as different from those of 80-Gy samples, whereas profiles from 20-Gy and 40-Gy samples were mostly transient between the two conditions. No structure was found to be unique and specific to a particular dose of irradiation. Among these structures, 20 species contained an *N*-glycolylneuraminic acid residue, 2 species contained an *N*-acetylneuraminic acid residue, and only 1 species contained both structures.

PCA of Measured MALDI-TOF Spectra—PCA was used as a descriptive approach in order to describe the glycomic dataset with exploratory statistics in response to irradiation (Fig. 6). It gave a simplified view of spectrum data in a two-component map for the control and irradiated samples. The data were analyzed either as a set of individual glycan structures (Fig. 6*A*) or as a set of glycan families (Fig. 6*B*). The resulting plots showed that the four sample sets clustered into two groups in a way that distinguished between the glycomic profiles derived from control and 20-Gy-irradiated animals and those of 40-Gy- and 80-Gy-irradiated animals. The discrimination was better for spectra data grouped in families, likely showing that changes involved sets of glycan structures rather than particular structures.

Mass Spectrometry Quantification of Structures and Glycan Families—Changes in the relative abundances of structure species and glycan families observed in glycosylation patterns between control and irradiated animals were determined using decisional statistics. One-way ANOVA and one-way ANOVA on ranks (Kruskal–Wallis) tests were used for the comparison of several series. All pairwise multiple comparison procedures (Tukey's test and Dunn's method) were used for the comparisons of series by pair. Relative to control

TABLE I

Assignment of molecular ions observed in the MALDI-MS spectra of permethylated N-glycans from blood serum of control and irradiated mice, and their putative structures

Mass (*m/z*)	Assignment (+ Na^+)	Family[a]	Putative structure[b]
1580 1784 1988 2192 2396	Hex5–9HexNAc2	High mannose glycans(Man family)	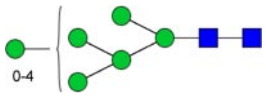
1795	Hex4HexNAc3dHex1	Monoantennary fucosylated glycan (BiFuc and F1 families)	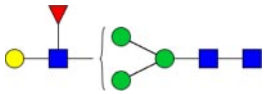
1836	Hex3HexNAc4dHex1	Biantennary fucosylated HexNAc-ended glycan (BiFuc, F1, and G0 families)	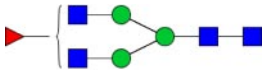
1999	Hex5HexNAc3dHex1	Hybrid fucosylated glycan (hybrid and F1 families)	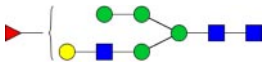
2012	Hex4HexNAc3NeuGc1	Monoantennary sialylated glycan (BiSia and S1 families)	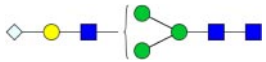
2040	Hex4HexNAc4dHex1	Biantennary fucosylated HexNAc-ended glycan (Bi Fuc, F1, and G0 families)	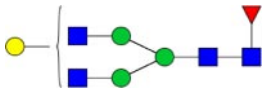
2216	Hex5HexNAc3NeuGc1	Hybrid sialylated glycan (hybrid and S1 families)	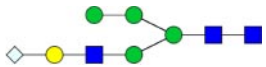
2244	Hex5HexNAc4dHex1	Biantennary fucosylated glycan (BiFuc and F1 families)	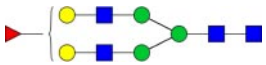
2257	Hex4HexNAc4NeuGc1	Biantennary sialylated HexNAc-ended glycan (BiSia, S1, and G0 families)	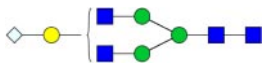
2420	Hex6HexNAc3NeuGc1	Hybrid sialylated glycan (hybrid and S1 families)	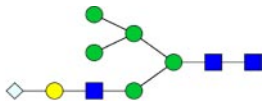
2448	Hex6HexNAc4dHex1	Biantennary fucosylated glycan (BiFuc and F1 families)	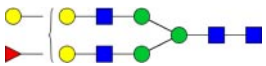
2461	Hex5HexNAc4NeuGc1	Biantennary sialylated glycan (BiSia and S1 families)	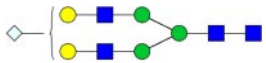
2607	Hex5HexNAc3NeuGc2	Hybrid disialylated glycan (hybrid and S2 families)	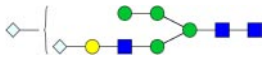
2635	Hex5HexNAc4NeuGc1dHex1	Biantennary sialylated and fucosylated glycan (BiFucSia, F1, and S1 families)	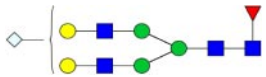

TABLE I—*continued*

Mass (*m/z*)	Assignment (+ Na^+)	Family[a]	Putative structure[b]
2796	Hex6HexNAc4dHex3	Biantennary trifucosylated glycan (BiFuc and F3 families)	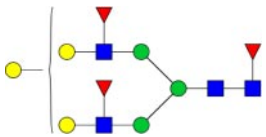
2809	Hex6HexNAc4NeuAc1dHex1	Biantennary sialylated and fucosylated glycan (BiFucSia, F2, and S1 families)	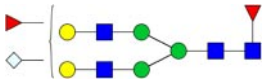
2822	Hex5HexNAc4NeuAc1NeuGc1	Biantennary disialylated glycan (BiSia and S2 families)	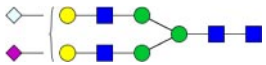
2837	Hex5HexNAc5dHex3	Triantennary trifucosylated HexNAc-ended glycan (TriFuc, F3, and G0 families)	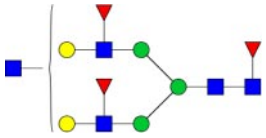
2852	Hex5HexNAc4NeuGc2	Biantennary disialylated glycan (BiSia and S2 families)	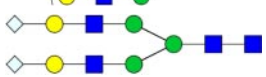
2867	Hex6HexNAc5dHex2	Hybrid fucosylated HexNAc-ended glycan (hybrid, F2, and G0 families)	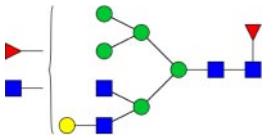
2895	Hex5HexNAc3NeuAc2dHex2	Hybrid fucosylated and sialylated glycan (hybrid, F2, and S2 families)	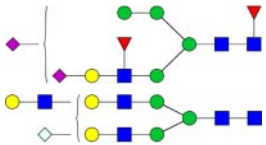
2910	Hex6HexNAc5NeuGc1	Triantennary sialylated glycan (TriSia and S1 families)	
3026	Hex5HexNAc4NeuGc2dHex1	Biantennary fucosylated and disialylated glycan (BiFucSia, F1, and S2 families)	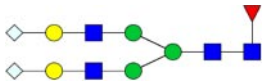
3056	Hex6HexNAc4NeuGc2	Biantennary disialylated glycan (BiSia and S2 families)	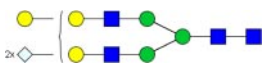
3228	Hex6HexNAc5NeuAc1dHex2	Triantennary difucosylated and sialylated glycan (TriFucSia, F2, and S1 families)	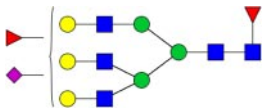
3244	Hex5HexNAc4NeuGc3	Biantennary trisialylated glycan (BiSia and S3 families)	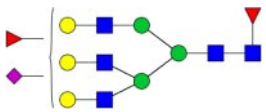
3259	Hex7HexNAc5NeuAc1dHex1	Triantennary fucosylated and sialylated glycan (TriFucSia, F2, and S1 families)	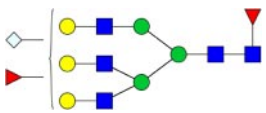

TABLE I—*continued*

Mass (*m/z*)	Assignment (+ Na^+)	Family[a]	Putative structure[b]
3288	Hex7HexNAc5NeuGc1dHex1	Triantennary fucosylated and sialylated glycan (TriFucSia, F1, and S1 families)	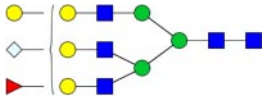
3302	Hex6HexNAc5NeuGc2	Triantennary disialylated glycan (TriSia and S2 families)	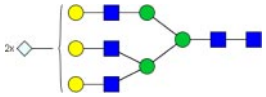
3635	Hex6HexNAc6dHex5	Tetraantennary pentafucosylated HexNAc-ended glycan (TetraFuc, F5, and G0 families)	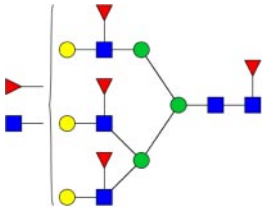
3663	Hex6HexNAc5NeuAc1NeuGc2	Triantennary fucosylated, HexNAc-ended trisialylated glycan (TriFucSia, F1, G0, and S3 families)	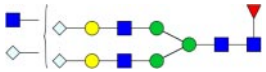
3678	Hex6HexNAc6NeuGc1dHex3	Tetraantennary trifucosylated and sialylated HexNAc-ended glycan (TetraFucSia, S1, F3, and G0 families)	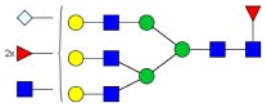
3693	Hex6HexNAc5NeuGc3	Triantennary trisialylated glycan (TriSia and S3 families)	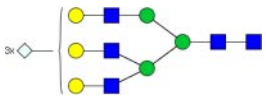
3708	Hex7HexNAc6NeuGc1dHex2	Tetraantennary difucosylated and sialylated glycan (TetraFucSia, F2, and S1 families)	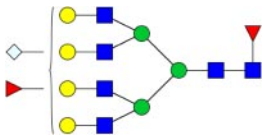
4084	Hex7HexNAc7dHex5	Tetraantennary pentafucosylated HexNAc-ended glycan (TetraFuc, F5, and G0 families)	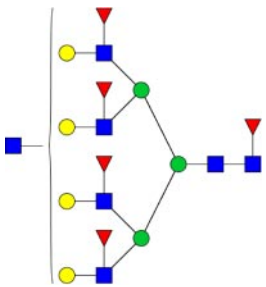

[a] Abbreviations of names of families are given in brackets.

[b] Putative structures were determined on the basis of composition, biosynthetic pathway knowledge, and MS/MS fragmentations. For convenience, only one branching pattern for triantennary structures and one branching pattern for hybrid structures are shown. Red triangles, fucose; yellow circles, galactose; green circles, mannose; blue squares, N-acetylglucosamine; pale blue rhomboids, *N*-glycolylneuraminic acid (sialic acid); purple rhomboids, *N*-acetylneuraminic acid (sialic acid).

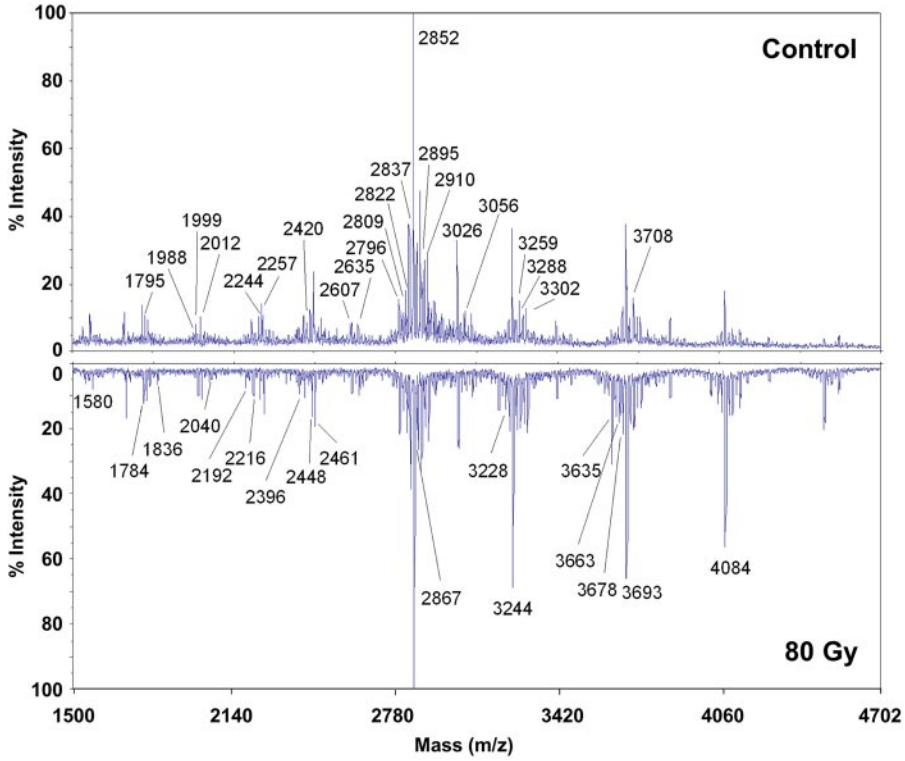

FIG. 5. **MALDI-TOF MS mirror spectra of permethylated *N*-glycans derived from sera of control and 80-Gy-irradiated mice.** Representative glycan map profiles of control and 80-Gy-irradiated mouse serum proteins are given and show qualitatively similar profiles but different peak intensities of the two samples. Each sample displays all the annotated signals, but the annotations were distributed on the two spectra for a more convenient reading of the figure. Changes in the relative abundances of structure species observed in glycosylation patterns between control and irradiated animals were further determined using decisional statistics (see Fig. 7).

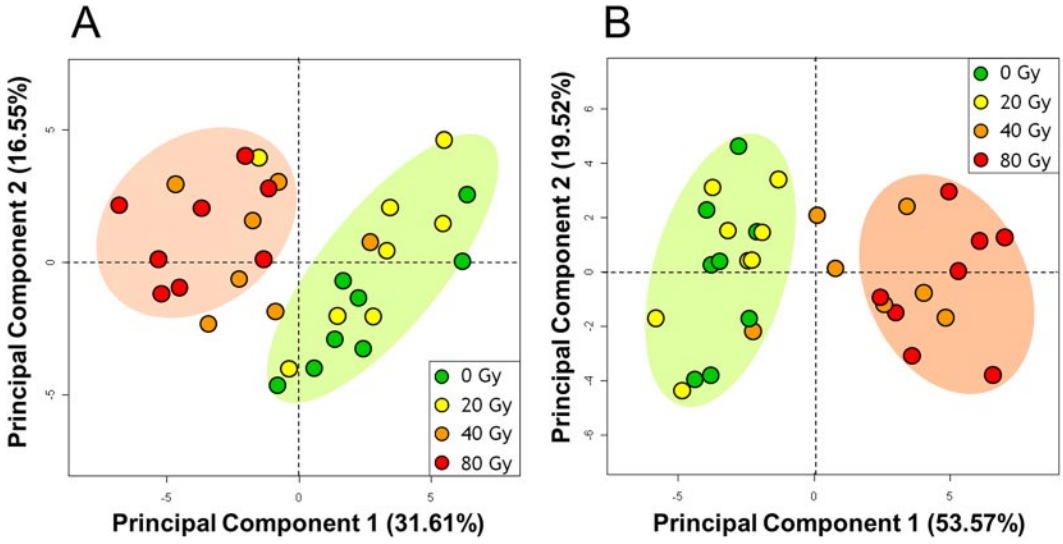

FIG. 6. **Principal component analysis of mass spectra of glycans derived from control mice (*n* = 8) and mice irradiated at 20 Gy (*n* = 8), 40 Gy (*n* = 7), and 80 Gy (*n* = 8).** *A*, glycan structures as variables. *B*, glycan families as variables.

samples, decreasing and increasing abundances of particular structures and families were observed with *p* values lower than 0.05 and with powers of tests higher than 80% (see supplemental Tables S3 and S4 for all statistical tests and expression fold change results). Fig. 7 shows histograms of the means of the relative amounts of glycan structures and glycan families that were significantly differentially expressed according to one-way ANOVA results. Statistically significant changes were observed for 15 glycan structures out of the 39 quantified in this study. Out of the 15 glycans, 9 were in-

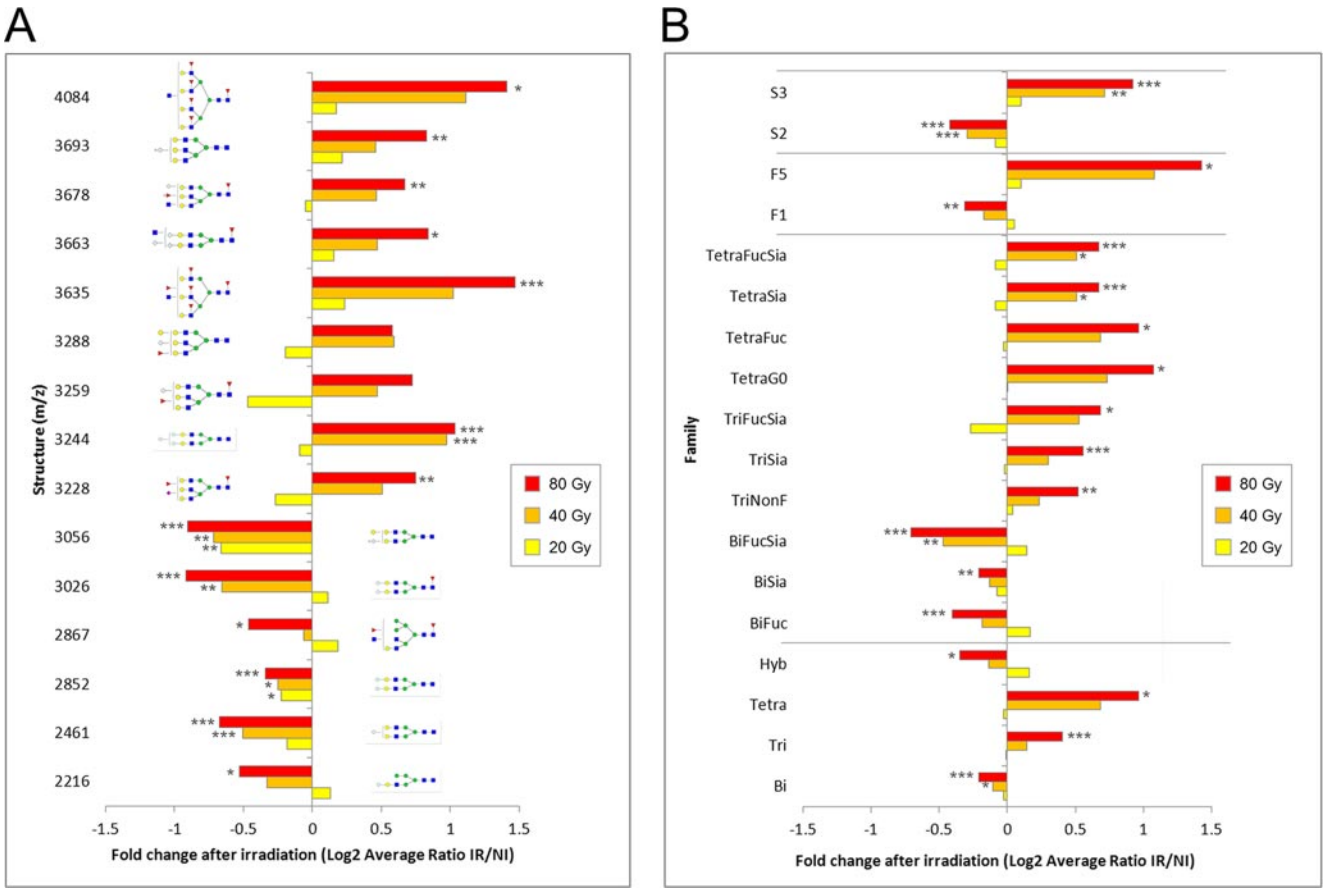

FIG. 7. **Changes in the relative intensities of significantly altered *N*-glycan structures and families derived from control mice ($n = 8$) and mice irradiated at 20 Gy ($n = 8$), 40 Gy ($n = 7$), and 80 Gy ($n = 8$) ($\log_2$ average ratio (IR/NI)).** *A*, glycan structures. *B*, glycan families. All statistical test results and expression fold changes are given in supplemental Tables S3 and S4. Abbreviations of family names are given in Table I. IR, irradiated samples; NI, non-irradiated samples. Asterisks indicate thresholds of the *p* value relative to the non-irradiated group: *, $p < 0.05$; **, $p < 0.01$; ***, $p < 0.001$. Red triangles, fucose; yellow circles, galactose; green circles, mannose; blue squares, *N*-acetylglucosamine; pale blue rhomboids, *N*-glycolylneuraminic acid (sialic acid); purple rhomboids, *N*-acetylneuraminic acid (sialic acid).

creased and 6 were decreased in the irradiated animal samples. 18 out of the 28 glycan families were significantly differentially expressed. *p* values and powers indicate that the differences were mostly statistically significant between control and 80-Gy samples and between 20- and 80-Gy samples (supplemental Tables S3 and S4, Fig. 7). A significant decrease of biantennary structures (*N*-glycans with *m/z* values of 2461, 2852, and 3026) occurred following exposure to the highest doses of irradiation (40 and 80 Gy), whereas an increase of almost all tri- and tetraantennary structures (*N*-glycans with *m/z* values of 3228, 3259, 3288, 3635, 3663, 3678, 3693, and 4084) took place at the same time. An increase was measured for the pentafucosylated glycan family (*N*-glycans with *m/z* values of 3635 and 4084). Similarly, an increase was observed for the S3 glycan family, which contains two different glycans with three sialic acid residues (*N*-glycans with *m/z* values of 3244 and 3693). In contrast, little difference was generally observed between control and 20 Gy and between 40 and 80 Gy, suggesting that control and 20-Gy-irradiated animals and 40- and 80-Gy-irradiated animals displayed similar responses at day 14 post-irradiation. These results agree with the findings we obtained using exploratory statistics with both two-dimensional DIGE and glycosylation profiles showing two main clusters, of control–20 Gy samples and of 40–80 Gy samples.

Expression Profiles of Liver Genes Involved in Glycosylation—Given that serum proteins are produced mainly in the liver, we wondered whether localized irradiation of the skin could induce changes in the expression of genes involved in glycosylation in this organ. Real-time quantitative PCR was used to evaluate changes in the relative abundances of 30 genes encoding fucosyltransferases (7 genes), acetylglucosaminyltransferases (GlcNAc transferases) (6 genes), galactosyltransferases (6 genes), and sialyltransferases (11 genes) (supplemental Tables S5 and S6, Fig. 8). The expression of four genes (MGAT5B, ABO, ST6GAL2, and ST6GALNAC5) was not detected in our conditions. Among the 26 detected genes, 17 were significantly differentially expressed in the liver at day 7 and/or day 14 post-irradiation at 80 Gy relative to sham-irradiated samples, showing that irradiation of the skin

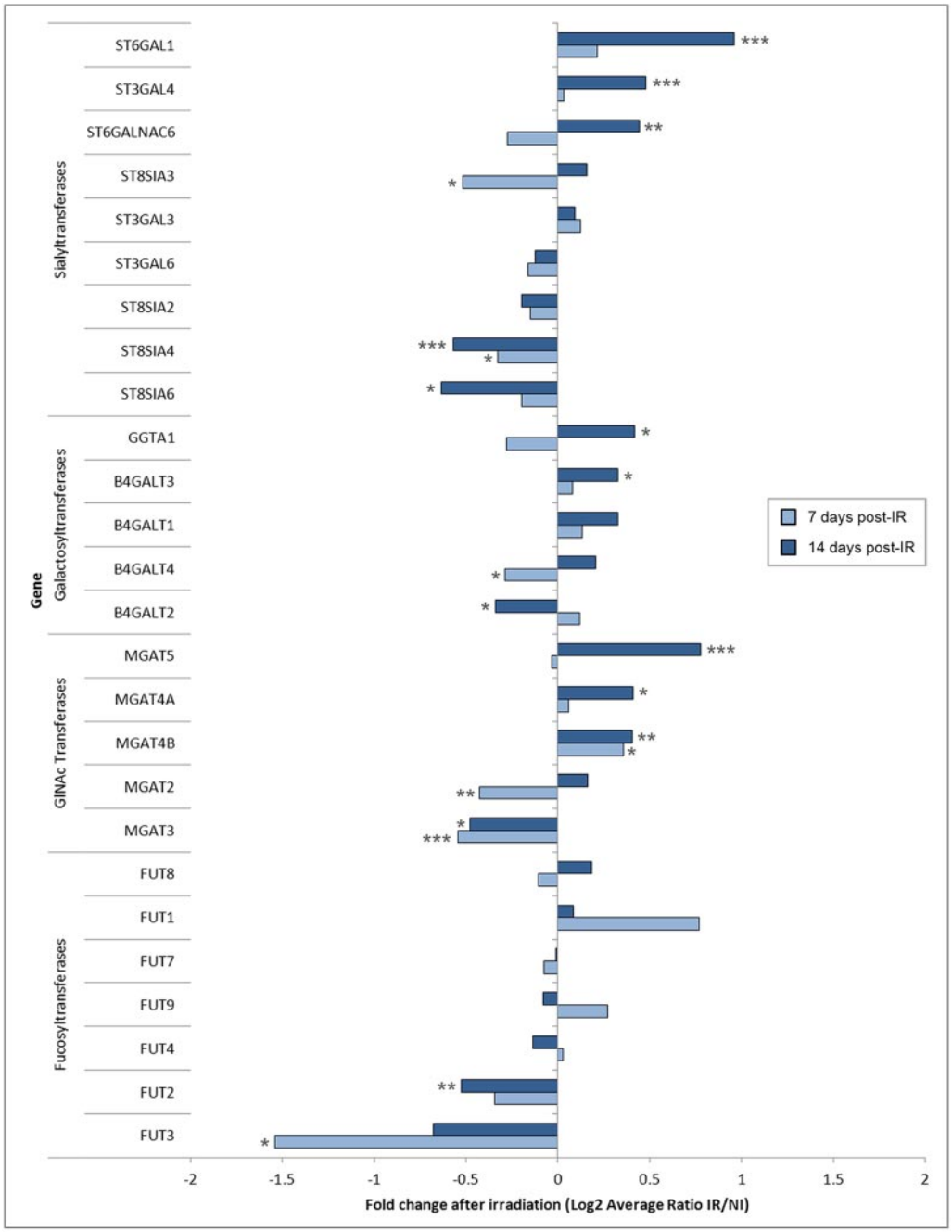

FIG. 8. **Irradiation of the skin induces changes in mRNA expression of genes involved in glycosylation in the liver.** Liver mRNA levels of fucosyltransferases, GlcNAc transferases, galactosyltransferases, and sialyltransferases were measured 7 and 14 days after irradiation at 80 Gy via real-time quantitative PCR (eight mice per time point) and were compared with corresponding mRNA levels of sham-irradiated mice ($n = 8$) ($\log_2$ average ratio (IR/NI)). IR, irradiated samples; NI, non-irradiated samples. Asterisks indicate thresholds of the p value relative to the non-irradiated group: *, $p < 0.05$; **, $p < 0.01$; ***, $p < 0.001$.

can broadly modify the expression of genes involved in glycosylation in the liver. Genes involved in the synthesis of multiantennary *N*-glycans (GlcNAc transferases MGAT4A, MGAT4B, and MGAT5) were overexpressed in the liver, particularly at day 14 post-irradiation. Furthermore, MGAT2, which produces the biantennary glycan substrates for the prior GlcNAc transferases, was not differentially expressed at day 14 post-irradiation. These findings correlate with the observed increase in multiantennary *N*-glycans of serum proteins. Similarly, the expression of genes involved in the sialylation of galactose (ST3GAL4 and ST6GAL1) and N-acetylglucosamine (ST6GALNAC6) were increased following irradiation, in line with the observed increase in outer branch sialylation of serum proteins after irradiation. In con-

trast, genes coding for sialyltransferases able to sialylate a sialic acid linked to galactose (ST8SIA3, ST8SIA4, ST8SIA6) were all down-regulated, but these findings were not in contradiction to the results of the glycomic study. In addition, we observed slight differential expression of several galactosyltransferase genes (B4GALT2, B4GALT3, B4GALT4, and GGTA1). Among these variations, the increase of GGTA1 might indicate an increase in the level of Galili antigen (Galα3Galβ4GlcNAc). Lastly, except for FUT2 and FUT3, which are responsible for the addition of a fucose to galactose, the expression of fucosyltransferase genes did not change significantly following irradiation, in apparent contradiction to the glycomic data, which revealed an increase in outer branch fucosylation. However, an increase in the synthesis of multiantennary structures induced by irradiation could lead to an increase in core and antenna fucosylation, even if genes are not expressed more, because antennary structures are able to accept fucose.

Quantification of Secreted Cytokines in Serum—The expression of genes involved in glycosylation can be regulated by proinflammatory cytokines expressed in the blood. We therefore looked for changes in the relative abundances of the three major proinflammatory cytokines, IL-1β, Il-6, and TNFα, in the serum of mice locally irradiated using a Luminex multiplexing assay. Fig. 9 shows that the three cytokines were significantly increased in the serum of mice at day 14 post-irradiation at 80 Gy relative to sham-irradiated mice. IL-6 was also significantly increased at day 7 post-irradiation and reached a maximum fold change of 2.5 at day 14. These results show that localized irradiation of the skin can significantly modify the level of blood proinflammatory cytokines, especially 14 days after the exposure. These cytokines might in turn change the expression of liver genes, as described in many studies, and especially the expression of genes involved in protein glycosylation.

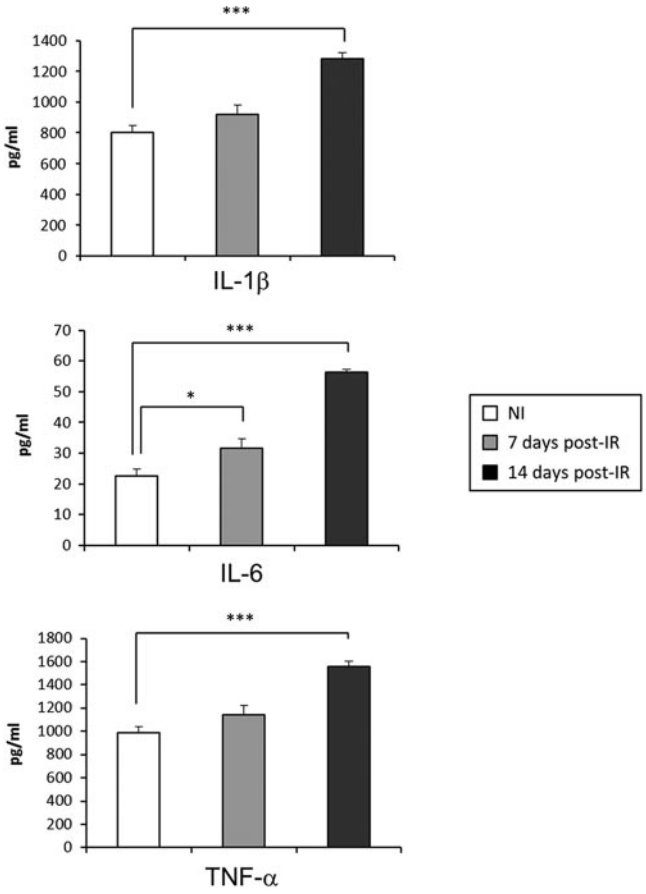

FIG. 9. **Irradiation of the skin induces changes in proinflammatory cytokines in the serum.** The levels of IL-1β, IL-6, and TNFα were measured 7 and 14 days after irradiation at 80 Gy (eight mice per time point) and in non-irradiated mice ($n = 8$) by the Luminex assay system (mean $\pm$ S.E.). Asterisks indicate thresholds of the p value relative to the non-irradiated group: *, $p < 0.05$; **, $p < 0.01$; ***, $p < 0.001$.

DISCUSSION

Research in our laboratory has validated an *in vivo* animal model of localized irradiation of the skin in order to shed light on CRS and to investigate serum protein changes before, during, and after the development of this syndrome (16, 33). Using this model, a first study to investigate time-course proteome changes showed that mice exhibited many differentially expressed serum proteins starting at 1 day following exposure to ionizing radiation and until 1 month post-irradiation (16). This response involved modifications in the abundance of acute phase response proteins and many other proteins of the serum, most of them known to be post-translationally modified. Based on a two-dimensional DIGE approach, shifts in the p*I* of serum proteins were observed in serum from irradiated animals, with a maximum shift at day 14 after irradiation, suggesting that modifications of proteins occurred in the serum of mice exposed to ionizing radiation and developing CRS.

In the present study, a proteomic analysis utilizing two-dimensional DIGE of the serum of a man irradiated by accident who was developing CRS at the time of blood collection (7) gave us the opportunity to observe similar shifts in the p*I* of human serum proteins during CRS. Observed in both humans and mice, these alterations might be of importance in the response to ionizing radiation. Because the first dimension of the procedure (isoelectric focusing) is exquisitely sensitive to molecular charge variations in sialic acid content (28), we investigated post-translational modification changes such as glycosylation in mouse after irradiation at 20, 40, and 80 Gy in the course of the development of CRS 14 days post-irradiation. Using exploratory statistics (PCA), comparisons of native and PNGase F–digested serum proteins via two-dimensional DIGE suggested that the large variations observed in the proteomic dataset between control and irradiated animals were mostly explained by glycosylated proteins. This result strongly supported the idea that glycosylation modifications of serum proteins explained, at least in part, the variation in

two-dimensional DIGE protein profiles after irradiation. Interestingly, PCA allowed the clustering of control and 20-Gy-irradiated animals and of 40- and 80-Gy-irradiated animals, showing good discrimination between uninjured/slightly injured animals and severely injured animals.

Because glycan modifications of protein amino acid side chains seemed to be important in the discrimination of mice exposed to different doses of ionizing radiation, we chose to explore the glycome of serum proteins in more detail using a mass spectrometry approach. We used in this study a small aliquot of 25 μl of unfractionated raw (non-depleted) serum from mouse to generate glycomic profiles through MALDI-MS. As discussed below, the data showed that local irradiation of the dorsal skin of mice significantly altered the glycome content of serum proteins in the course of the development of the radiation-induced lesion.

A significant decrease of biantennary structures occurred following exposure to the highest doses of irradiation (40 and 80 Gy), whereas an increase of almost all tri- and tetraantennary glycans took place at the same time. This result is in agreement with previous work establishing that in cancer or other chronic inflammation states, the increase in tri- and tetraantennary glycans signals chronic inflammation (22). Furthermore, we established that the mRNA levels of genes involved in the synthesis of multiantennary structures (MGAT4A, MGTA4B, and MGAT5) were increased in the liver of irradiated mice relative to sham-irradiated mice. As serum proteins are produced mainly in the liver, the observed decreases in biantennary *N*-glycans and increases in multiantennary *N*-glycans might result at least in part from an alteration of N-GlcNAc expression. These results should be confirmed via Western blot analysis and protein activity assays. The synthesis of multiantennary structures has been shown to be greatly modulated during the inflammatory process, and various studies have associated such variations with sialylation and fucosylation and, more specifically, with the Sle^X epitope (22). In the present study, the assessment of the levels the three key proinflammatory cytokines, IL-1β, IL-6, and TNFα, in the serum of irradiated mice demonstrated that an inflammatory reaction was occurring at the time of the glycomic study. Lastly, in contrast to the decrease we observed in the full biantennary glycan family, α1-acid glycoprotein was shown to contain increasing amounts of biantennary structures during short-term acute inflammation (39), but this result cannot easily be generalized to the full biantennary glycan family. Moreover, mice could instead exhibit chronic inflammation, which is characteristic of the long-term effect of irradiation (40).

An increase in the pentafucosylated glycan family was measured in irradiated mice. This increase was not supported by an up-regulation of fucosyltransferase genes in the liver. However, an increase in the synthesis of multiantennary structures induced by irradiation could be sufficient to explain an increase in fucosylation, even if fucosyltransferase genes were not up-regulated, because antennary structures are able to accept fucose. The pentafucosylated family of glycans is composed of hyperfucosylated structures that were not sialylated in our experiment and which, as a consequence, likely did not carry the Sle^X epitope. The Sle^X epitope has a role in inflammation when linked to cellular glycoproteins (41), but it has also been found to be increased on serum APPs during chronic pancreatitis (42). However, the physiological role of increased branching and SLe^x on serum glycoproteins remains elusive. If confirmed, the contradictory result we obtained might account for the specificity of the radiation effect in regard to other pathologies, such as cancer and organ inflammation.

Similarly, an increase was observed in the S3 glycan family, which contains three sialic acid residues. These changes might explain the observed shifts of spot trains toward acidic pH levels in two-dimensional DIGE in our previous work (16) and for both mouse and human serum proteins in this study. In accordance with our results, a total increase in sialylation has been observed when an acute phase response was induced in mice via turpentine oil injection (27, 43). Moreover, increased sialylation was related to the production of the proinflammatory cytokine IL-6 in patients with cystic fibrosis (44) and in patients with gastric cancer (45). Interestingly, IL-6 is one of the major cytokines involved in the response to ionizing radiation, especially in skin (13, 14, 46). In the present study, IL-6 was significantly increased in the serum 7 and 14 days post-irradiation of the skin, and IL-1β and TNFα were increased at day 14. Moreover, the mRNA levels of sialyltransferases (ST3GAL4, ST6GAL1, and ST6GALNAC6) were up-regulated in the liver at day 14 post-irradiation. Furthermore, ST6GAL1, which is highly expressed in the liver (47), has been shown to be up-regulated by IL-6 (48) and TNFα (49, 50), and the expression of ST3GAL4 was increased by IL-1β (51). An induction of IL-1β, IL-6, and TNFα following irradiation of the skin might therefore explain the observed increase in serum sialylated glycans after radiation exposure.

No information was available to explain changes in glycome content following irradiation. It is not known whether they were caused by increases in the abundance of modified proteins with these particular structures or by increases in particular structures linked to different proteins, as can be seen when there is an increase of the expression of glycosyltransferases (52). However, the up-regulation of genes involved in glycosylation in the liver of locally irradiated mice indicates that the glycome content might be modified at least in part by the increase in particular structures. In the current work we present no new experimental data about the identities of modified serum glycoproteins after irradiation. However, we have shown previously that contrapsin, carboxylesterase, gelsolin, kininogen I, hemopexin, Pzp, complement component C3, and α1-antitrypsin, which form spot trains on two-dimensional gels, were likely post-translationally modified after irradiation (16). We hypothesized that irradiation modified

their glycosylation status. In this paper, we focus on the modifications of a spot train that was identified as contrapsin (serpin 3K) in that same earlier study. These modifications occurred in a dose-dependent manner, and the contrapsin spot train disappeared from two-dimensional gels when serum proteins were treated with PNGase F. All these spot trains were shifted mostly toward acidic pH levels following irradiation, with a maximum shift at day 14. Given that many proteins in serum are modified by sialic acid chains, giving rise to characteristic spot trains on a two-dimensional gel (28), the changes we observed might be due mainly to an increase in the sialic acid content of glycans linked to these proteins, except for gelsolin, which shifted toward basic pH levels after irradiation. All these proteins, with the exception of gelsolin, are consistent with the acute phase response to tissue injury. Many APPs are heavily glycosylated, and their sugar content and complexity can change, for instance, in the presence of cancer-induced chronic inflammation (53). These changes in glycosylation can profoundly alter the function of a protein and are likely involved in the processes of inflammation and tissue repair. Although almost all proteins we identified on two-dimensional gels in our first study were linked to the acute phase response, the specificity of the response to some proteins remains an open question. Another interesting question is the potential reversibility of this serum glycoprotein phenotype after radiation treatment. We showed that profiles of spot trains returned to values similar to those of sham-irradiated mice in about 1 month (16), indicating that this phenotype might be reversible. However, this question still deserves to be explored, as the serum glycome was not investigated beyond 14 days after irradiation.

The observed increases in multiantennary *N*-glycans and in outer branch fucosylation and sialylation were associated with the up-regulation of genes involved in glycosylation in the liver, which is the main producer of serum proteins, and with an increase in key proinflammatory serum cytokines, which can be involved in the control of the expression of glycosylation genes. We hypothesize that radiation-induced skin lesions induce the release of cytokines in the circulation, which in turn might lead to altered expression of liver genes involved in the glycosylation of proteins, giving rise to modifications of secreted protein glycosylation status. The molecular background and physiological importance of most of these changes, however, remain to be discovered. Changes in the glycosylation of serum proteins have clearly shown that glycosylation plays an important role in the inflammatory response (27). Changes in the sialylation and fucosylation of APPs can induce the increased expression of structures involved in the selectin-mediated interaction of leukocytes and endothelial cells in homing and inflammatory processes (54). It has been postulated that the inflammation-induced changes in the expression of these structure on APPs might have an inhibitory effect on the selectin-mediated entry of leukocytes into inflamed areas (41, 55, 56) and might represent a feedback response of the hepatic acute phase reaction in an attempt to reduce the cellular inflammatory reaction. Further identification of proteins whose glycosylation might be modified following irradiation therefore remains a challenge in elucidating the molecular and cellular events involved in the response to ionizing radiation.

CONCLUSIONS

MS-based glycomic profiles have clearly demonstrated that changes occur in the relative abundances of many glycan structures and glycan families of serum proteins following irradiation. The observed decreases in biantennary *N*-glycans and increases in multiantennary *N*-glycans, as well as increases in outer branch fucosylation, are reminiscent of the types of alterations observed previously following inflammatory stimuli. This probably also takes place in humans, as serum proteins of a man exposed to ionizing radiation and developing CRS displayed two-dimensional DIGE patterns similar to those of mouse samples. Using glycan structures as variables, PCA of the control and irradiated groups of samples demonstrated a clear clustering between control and 20-Gy samples and between 40- and 80-Gy samples. These results show that glycomic profiling has the potential to discriminate between uninjured/slightly injured animals (control and 20 Gy) and severely injured animals (40 and 80 Gy). This methodology might be the starting point for the development of new categories of radiation diagnostic or prognostic biomarkers based on the quantification of glycan structures in serum. As with serum proteome studies designed to identify prognostic and diagnostic biomarkers, the investigation of the temporal expression of glycans will have to be considered, especially during the latent phase following exposure. Characterizing the global molecular consequences of ionizing radiation remains a challenge, especially for localized injury following high doses of radiation. Finally, a more comprehensive picture of the pathophysiological response to localized radiation exposure is still needed for better clinical triage when there are mass casualties, and to predict lesion outcomes for each patient.

Acknowledgments—We thank Dr. Anne-Sophie Vercoutter-Edouart (UGSF, Lille) and Dr. David Marsh for correcting the manuscript. We are also grateful to Dr. Anne Harduin-Lepers (UGSF, Lille) for her expertise and advice on glycosyltransferase genes and to Dr. Yann Guerardel (UGSF, Lille) for his help in MS/MS spectra interpretations.

* The research leading to these results has received funding from Electricité de France (Groupe Gestion Projet - Radioprotection) and from the European Union's Seventh Framework Programme (FP7/2007–2013) under Grant Agreement No. 241536.

S This article contains supplemental material.

‡‡ To whom correspondence should be addressed: Olivier Guipaud, Institut de Radioprotection et de Sûreté Nucléaire (IRSN), DRPH, SRBE, LRTE, 31 avenue de la Division Leclerc, 92260 Fontenay-aux-Roses, France, Tel.: 33 1 58 35 70 53, Fax: 33 1 58 35 84 67, E-mail: olivier.guipaud@irsn.fr.

§ These authors contributed equally to this work.

REFERENCES

1. Hopewell, J. W. (1990) The skin: its structure and response to ionizing radiation. *Int. J. Radiat. Biol.* **57,** 751–773
2. Gottlober, P., Bezold, G., Weber, L., Gourmelon, P., Cosset, J. M., Bahren, W., Hald, H. J., Fliedner, T. M., and Peter, R. U. (2000) The radiation accident in Georgia: clinical appearance and diagnosis of cutaneous radiation syndrome. *J. Am. Acad. Dermatol.* **42,** 453–458
3. Peter, R. U., Steinert, M., and Gottlober, P. (2001) The cutaneous radiation syndrome: diagnosis and treatment. *Radioprotection* **49,** 451–457
4. Muller, K., and Meineke, V. (2010) Advances in the management of localized radiation injuries. *Health Phys.* **98,** 843–850
5. Meineke, V. (2005) The role of damage to the cutaneous system in radiation-induced multi-organ failure. *Br. J. Radiol. Suppl.* **27,** 85–99
6. Ainsbury, E. A., Bakhanova, E., Barquinero, J. F., Brai, M., Chumak, V., Correcher, V., Darroudi, F., Fattibene, P., Gruel, G., Guclu, I., Horn, S., Jaworska, A., Kulka, U., Lindholm, C., Lloyd, D., Longo, A., Marrale, M., Monteiro Gil, O., Oestreicher, U., Pajic, J., Rakic, B., Romm, H., Trompier, F., Veronese, I., Voisin, P., Vral, A., Whitehouse, C. A., Wieser, A., Woda, C., Wojcik, A., and Rothkamm, K. (2010) Review of retrospective dosimetry techniques for external ionising radiation exposures. *Radiat. Prot. Dosimetry* **147,** 573–592
7. Lataillade, J. J., Doucet, C., Bey, E., Carsin, H., Huet, C., Clairand, I., Bottollier-Depois, J. F., Chapel, A., Ernou, I., Gourven, M., Boutin, L., Hayden, A., Carcamo, C., Buglova, E., Joussemet, M., de Revel, T., and Gourmelon, P. (2007) New approach to radiation burn treatment by dosimetry-guided surgery combined with autologous mesenchymal stem cell therapy. *Regen. Med.* **2,** 785–794
8. Bey, E., Prat, M., Duhamel, P., Benderitter, M., Brachet, M., Trompier, F., Battaglini, P., Ernou, I., Boutin, L., Gourven, M., Tissedre, F., Crea, S., Mansour, C. A., de Revel, T., Carsin, H., Gourmelon, P., and Lataillade, J. J. (2010) Emerging therapy for improving wound repair of severe radiation burns using local bone marrow-derived stem cell administrations. *Wound Repair Regen.* **18,** 50–58
9. Akita, S., Akino, K., Hirano, A., Ohtsuru, A., and Yamashita, S. (2010) Mesenchymal stem cell therapy for cutaneous radiation syndrome. *Health Phys.* **98,** 858–862
10. Benderitter, M., Gourmelon, P., Bey, E., Chapel, A., Clairand, I., Prat, M., and Lataillade, J. J. (2010) New emerging concepts in the medical management of local radiation injury. *Health Phys.* **98,** 851–857
11. Guipaud, O., and Benderitter, M. (2009) Protein biomarkers for radiation exposure: towards a proteomic approach as a new investigation tool. *Ann. Ist. Super. Sanita* **45,** 278–286
12. Tapio, S., Hornhardt, S., Gomolka, M., Leszczynski, D., Posch, A., Thalhammer, S., and Atkinson, M. J. (2010) Use of proteomics in radiobiological research: current state of the art. *Radiat. Environ. Biophys.* **49,** 1–4
13. Barcellos-Hoff, M. H. (1998) How do tissues respond to damage at the cellular level? The role of cytokines in irradiated tissues. *Radiat. Res.* **150,** S109-S120
14. Muller, K., and Meineke, V. (2007) Radiation-induced alterations in cytokine production by skin cells. *Exp. Hematol.* **35,** 96–104
15. Gabay, C., and Kushner, I. (1999) Acute-phase proteins and other systemic responses to inflammation. *N. Engl. J. Med.* **340,** 448–454
16. Guipaud, O., Holler, V., Buard, V., Tarlet, G., Royer, N., Vinh, J., and Benderitter, M. (2007) Time-course analysis of mouse serum proteome changes following exposure of the skin to ionizing radiation. *Proteomics* **7,** 3992–4002
17. Rudd, P. M., and Dwek, R. A. (1997) Glycosylation: heterogeneity and the 3D structure of proteins. *Crit. Rev. Biochem. Mol. Biol.* **32,** 1–100
18. Apweiler, R., Hermjakob, H., and Sharon, N. (1999) On the frequency of protein glycosylation, as deduced from analysis of the SWISS-PROT database. *Biochim. Biophys. Acta* **1473,** 4–8
19. Dube, D. H., and Bertozzi, C. R. (2005) Glycans in cancer and inflammation—potential for therapeutics and diagnostics. *Nat. Rev. Drug Discov.* **4,** 477–488
20. Tian, Y., and Zhang, H. (2010) Glycoproteomics and clinical applications. *Proteomics Clin. Appl.* **4,** 124–132
21. Kyselova, Z., Mechref, Y., Al Bataineh, M. M., Dobrolecki, L. E., Hickey, R. J., Vinson, J., Sweeney, C. J., and Novotny, M. V. (2007) Alterations in the serum glycome due to metastatic prostate cancer. *J. Proteome Res.* **6,** 1822–1832
22. Arnold, J. N., Saldova, R., Hamid, U. M., and Rudd, P. M. (2008) Evaluation of the serum N-linked glycome for the diagnosis of cancer and chronic inflammation. *Proteomics* **8,** 3284–3293
23. Arnold, J. N., Saldova, R., Galligan, M. C., Murphy, T. B., Mimura-Kimura, Y., Telford, J. E., Godwin, A. K., and Rudd, P. M. (2011) Novel glycan biomarkers for the detection of lung cancer. *J. Proteome Res.* **10,** 1755–1764
24. Bones, J., Byrne, J. C., O'Donoghue, N., McManus, C., Scaife, C., Boissin, H., Nastase, A., and Rudd, P. M. (2011) Glycomic and glycoproteomic analysis of serum from patients with stomach cancer reveals potential markers arising from host defense response mechanisms. *J. Proteome Res.* **10,** 1246–1265
25. Morelle, W., and Michalski, J. C. (2007) Analysis of protein glycosylation by mass spectrometry. *Nat. Protoc.* **2,** 1585–1602
26. Pabst, M., and Altmann, F. (2011) Glycan analysis by modern instrumental methods. *Proteomics* **11,** 631–643
27. Gornik, O., and Lauc, G. (2008) Glycosylation of serum proteins in inflammatory diseases. *Dis. Markers* **25,** 267–278
28. Anderson, N. L., and Anderson, N. G. (2002) The human plasma proteome: history, character, and diagnostic prospects. *Mol. Cell. Proteomics* **1,** 845–867
29. Ciucanu, I., and Kerek, F. (1984) A simple and rapid method for the permethylation of carbohydrates. *Carbohydr. Res.* **131,** 209–217
30. Ceroni, A., Dell, A., and Haslam, S. M. (2007) The GlycanBuilder: a fast, intuitive and flexible software tool for building and displaying glycan structures. *Source Code Biol. Med.* **2,** 3
31. Ranzinger, R., Herget, S., von der Lieth, C. W., and Frank, M. (2011) GlycomeDB—a unified database for carbohydrate structures. *Nucleic Acids Res.* **39,** D373-D376
32. Lê, S., Josse, J., and Husson, F. (2008) FactoMineR: an R package for multivariate analysis. *J. Stat. Soft.* **25,** 1–18
33. Holler, V., Buard, V., Gaugler, M. H., Guipaud, O., Baudelin, C., Sache, A., Perez Mdel, R., Squiban, C., Tamarat, R., Milliat, F., and Benderitter, M. (2009) Pravastatin limits radiation-induced vascular dysfunction in the skin. *J. Invest. Dermatol.* **129,** 1280–1291
34. Wada, Y., Azadi, P., Costello, C. E., Dell, A., Dwek, R. A., Geyer, H., Geyer, R., Kakehi, K., Karlsson, N. G., Kato, K., Kawasaki, N., Khoo, K. H., Kim, S., Kondo, A., Lattova, E., Mechref, Y., Miyoshi, E., Nakamura, K., Narimatsu, H., Novotny, M. V., Packer, N. H., Perreault, H., Peter-Katalinic, J., Pohlentz, G., Reinhold, V. N., Rudd, P. M., Suzuki, A., and Taniguchi, N. (2007) Comparison of the methods for profiling glycoprotein glycans—HUPO Human Disease Glycomics/Proteome Initiative multi-institutional study. *Glycobiology* **17,** 411–422
35. Albrethsen, J. (2007) Reproducibility in protein profiling by MALDI-TOF mass spectrometry. *Clin. Chem.* **53,** 852–858
36. Molloy, M. P., Brzezinski, E. E., Hang, J., McDowell, M. T., and VanBogelen, R. A. (2003) Overcoming technical variation and biological variation in quantitative proteomics. *Proteomics* **3,** 1912–1919
37. Molloy, M. P., Donohoe, S., Brzezinski, E. E., Kilby, G. W., Stevenson, T. I., Baker, J. D., Goodlett, D. R., and Gage, D. A. (2005) Large-scale evaluation of quantitative reproducibility and proteome coverage using acid cleavable isotope coded affinity tag mass spectrometry for proteomic profiling. *Proteomics* **5,** 1204–1208
38. Whistler, T., Rollin, D., and Vernon, S. D. (2007) A method for improving SELDI-TOF mass spectrometry data quality. *Proteome Sci.* **5,** 14
39. Fassbender, K., Zimmerli, W., Kissling, R., Sobieska, M., Aeschlimann, A., Kellner, M., and Muller, W. (1991) Glycosylation of alpha 1-acid glycoprotein in relation to duration of disease in acute and chronic infection and inflammation. *Clin. Chim. Acta* **203,** 315–327
40. Robbins, M. E., and Zhao, W. (2004) Chronic oxidative stress and radiation-induced late normal tissue injury: a review. *Int. J. Radiat. Biol.* **80,** 251–259
41. Phillips, M. L., Nudelman, E., Gaeta, F. C., Perez, M., Singhal, A. K., Hakomori, S., and Paulson, J. C. (1990) ELAM-1 mediates cell adhesion by recognition of a carbohydrate ligand, sialyl-Lex. *Science* **250,** 1130–1132
42. Sarrats, A., Saldova, R., Pla, E., Fort, E., Harvey, D. J., Struwe, W. B., de Llorens, R., Rudd, P. M., and Peracaula, R. (2010) Glycosylation of liver acute-phase proteins in pancreatic cancer and chronic pancreatitis. *Proteomics Clin. Appl.* **4,** 432–448
43. Chavan, M. M., Kawle, P. D., and Mehta, N. G. (2005) Increased sialylation

and defucosylation of plasma proteins are early events in the acute phase response. *Glycobiology* **15,** 838–848
44. Groux-Degroote, S., Krzewinski-Recchi, M. A., Cazet, A., Vincent, A., Lehoux, S., Lafitte, J. J., Van Seuningen, I., and Delannoy, P. (2008) IL-6 and IL-8 increase the expression of glycosyltransferases and sulfotransferases involved in the biosynthesis of sialylated and/or sulfated Lewisx epitopes in the human bronchial mucosa. *Biochem. J.* **410,** 213–223
45. Ikeguchi, M., Hatada, T., Yamamoto, M., Miyake, T., Matsunaga, T., Fukumoto, Y., Yamada, Y., Fukuda, K., Saito, H., and Tatebe, S. (2009) Serum interleukin-6 and -10 levels in patients with gastric cancer. *Gastric Cancer* **12,** 95–100
46. Benderitter, M., Isoir, M., Buard, V., Durand, V., Linard, C., Vozenin-Brotons, M. C., Steffanazi, J., Carsin, H., and Gourmelon, P. (2007) Collapse of skin antioxidant status during the subacute period of cutaneous radiation syndrome: a case report. *Radiat. Res.* **167,** 43–50
47. Kitagawa, H., and Paulson, J. C. (1994) Differential expression of five sialyltransferase genes in human tissues. *J. Biol. Chem.* **269,** 17872–17878
48. Naugler, W. E., Sakurai, T., Kim, S., Maeda, S., Kim, K., Elsharkawy, A. M., and Karin, M. (2007) Gender disparity in liver cancer due to sex differences in MyD88-dependent IL-6 production. *Science* **317,** 121–124
49. Hanasaki, K., Varki, A., and Powell, L. D. (1995) CD22-mediated cell adhesion to cytokine-activated human endothelial cells. Positive and negative regulation by alpha 2–6-sialylation of cellular glycoproteins. *J. Biol. Chem.* **270,** 7533–7542
50. Hanasaki, K., Varki, A., Stamenkovic, I., and Bevilacqua, M. P. (1994) Cytokine-induced beta-galactoside alpha-2,6-sialyltransferase in human endothelial cells mediates alpha 2,6-sialylation of adhesion molecules and CD22 ligands. *J. Biol. Chem.* **269,** 10637–10643
51. Higai, K., Miyazaki, N., Azuma, Y., and Matsumoto, K. (2006) Interleukin-1beta induces sialyl Lewis X on hepatocellular carcinoma HuH-7 cells via enhanced expression of ST3Gal IV and FUT VI gene. *FEBS Lett.* **580,** 6069–6075
52. Yasukawa, Z., Sato, C., and Kitajima, K. (2005) Inflammation-dependent changes in alpha2,3-, alpha2,6-, and alpha2,8-sialic acid glycotopes on serum glycoproteins in mice. *Glycobiology* **15,** 827–837
53. Dempsey, E., and Rudd, P. M. (2012) Acute phase glycoproteins: bystanders or participants in carcinogenesis? *Ann. N. Y. Acad. Sci.* **1253,** 122–132
54. Lasky, L. A. (1992) Selectins: interpreters of cell-specific carbohydrate information during inflammation. *Science* **258,** 964–969
55. De Graaf, T. W., Van der Stelt, M. E., Anbergen, M. G., and van Dijk, W. (1993) Inflammation-induced expression of sialyl Lewis X-containing glycan structures on alpha 1-acid glycoprotein (orosomucoid) in human sera. *J. Exp. Med.* **177,** 657–666
56. Walz, G., Aruffo, A., Kolanus, W., Bevilacqua, M., and Seed, B. (1990) Recognition by ELAM-1 of the sialyl-Lex determinant on myeloid and tumor cells. *Science* **250,** 1132–1135